THE JOURNAL OF PHYSICAL CHEMISTRY B

Article

Cite This: J. Phys. Chem. B 2019, 123, 10131−10141

pubs.acs.org/JPCB

Trajectory-Based Simulation of EPR Spectra: Models of Rotational Motion for Spin Labels on Proteins

Peter D. Martin,[†,‡] Bengt Svensson,[†] David D. Thomas,*[,†,‡] and Stefan Stoll*[,§]

[†]Department of Biochemistry, Molecular Biology, and Biophysics and [‡]School of Physics and Astronomy, University of Minnesota, Minneapolis, Minnesota 55455, United States

[§]Department of Chemistry, University of Washington, Seattle, Washington 98195, United States

Supporting Information

ABSTRACT: Direct time-domain simulation of continuous-wave (CW) electron paramagnetic resonance (EPR) spectra from molecular dynamics (MD) trajectories has become increasingly popular, especially for proteins labeled with nitroxide spin labels. Due to the time-consuming nature of simulating adequately long MD trajectories, two approximate methods have been developed to reduce the MD-trajectory length required for modeling EPR spectra: hindered Brownian diffusion (HBD) and hidden Markov models (HMMs). Here, we assess the accuracy of these two approximate methods relative to direct simulations from MD trajectories for three spin-labeled protein systems (a simple helical peptide, a soluble protein, and a membrane protein) and two nitroxide spin labels with differing mobilities (R1 and 2,2,6,6-tetramethylpiperidine-1-oxyl-4-amino-4-carboxylic acid (TOAC)). We find that the HMMs generally outperform HBD. Although R1 dynamics partially resembles hindered Brownian diffusion, HMMs accommodate the multiple dynamic time scales for the transitions between rotameric states of R1 that cannot be captured accurately by a HBD model. The MD trajectories of the TOAC-labeled proteins show that its dynamics closely resembles slow multisite exchange between twist-boat and chair ring puckering states. This motion is modeled well by HMM but not by HBD. All MD-trajectory data processing, stochastic trajectory simulations, and CW EPR spectral simulations are implemented in EasySpin, a free software package for MATLAB.

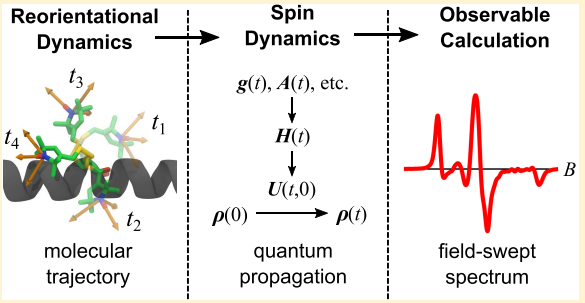

INTRODUCTION

Electron paramagnetic resonance (EPR) spectroscopy can reveal local, quantitative information about protein dynamics and structure. By performing site-directed spin labeling,[1,2] where a paramagnetic "spin label" is attached to or incorporated into the backbone of a host protein, one can measure a protein's rotational dynamics, conformational changes, accessibility to solvent or lipid bilayers, and much more. However, since the EPR spectrum reflects the behavior of both the spin label and the host protein, it can be complex and difficult to interpret. Accurate modeling of the spin label, the protein, and their surrounding environment is essential for extracting detailed structural and dynamic information from the EPR spectrum.

The primary difficulty in simulating continuous-wave (CW) EPR spectra of spin-labeled proteins is that the time scale of the spatial molecular dynamics (≈0.1−10 ns at room temperature) is comparable to the inverse of the spectral anisotropy (the maximum change in resonance line positions as the spin-label orientation is varied). In this regime, both spatial molecular dynamics and quantum spin dynamics need to be treated on the same footing. Some early developments in this area focused on perturbational calculations[3,4] and diffusion-coupled Bloch equations[5,6] to simulate EPR spectra. However, the dominant method for tackling this problem has been to simulate EPR spectra using a simple rigid-body hindered Brownian diffusion model (HBD), solving the associated stochastic Liouville equation (SLE) in the frequency domain via an eigenfunction expansion, and fitting the model parameters to experimental data.[7−11] Existing programs[12,13] that perform this task are very fast, and the method has been of immense value in many structural and dynamic studies. However, the model is extremely simplistic and is not able to fully capture the multistate and multitimescale structural dynamics of the spin label and its environment. Additionally, these programs are limited to nitroxides, but several spin labels other than nitroxide radicals have been increasingly employed (Gd^{3+},[14] Cu^{2+},[15] triarylmethyl[16]). To model spectra with these labels and more complex label-environment interactions, more general methods are required. As a result, there has been growing interest in obtaining EPR spectra of spin-labeled proteins directly from molecular dynamics (MD) or other time-domain trajectories.[17−41]

This time-domain approach utilizes dynamical orientational trajectories of the paramagnetic spin system to calculate the time-dependent magnetization after a 90° pulse, i.e., the free-

Received: March 21, 2019
Revised: October 7, 2019
Published: November 6, 2019

DOI: 10.1021/acs.jpcb.9b02693
J. Phys. Chem. B 2019, 123, 10131−10141

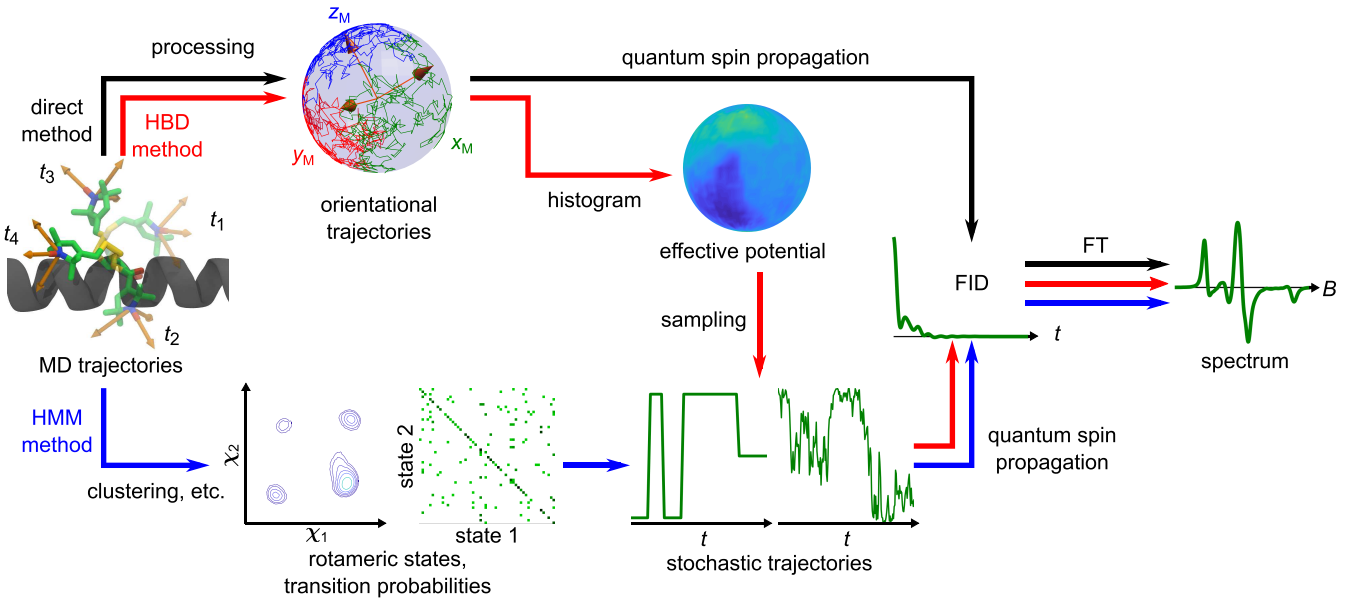

Figure 1. Flow chart depicting the different time-domain simulation methods and their hierarchy. HBD: hindered Brownian diffusion, HMM: hidden Markov model, FID: free-induction decay, FT: Fourier transformation.

induction decay (FID), then perform a Fourier transformation and scale the frequency axis to obtain the field-swept CW spectrum. This approach is attractive because it can accommodate motional models of arbitrary complexity, anywhere between simple rigid-body Brownian diffusion and all-atom MD trajectories.

The primary aim of this paper is to compare several MD-trajectory-based methods of EPR spectral simulation (see Figure 1). The simplest method is to directly use the MD trajectory to model the motion of the spin label and calculate the time-dependent FID (direct method, black).[28,33] In this approach, a sufficient number of MD trajectories of adequate length need to be calculated to result in a converged simulated EPR spectrum. However, a typical FID can last several hundred nanoseconds and, at present, it would be prohibitive to simulate many MD trajectories of this length, which require time steps on the order of 1 fs to accurately model molecular motion and interactions. As a result, two approximate spectral simulation methods were developed that reduce the required MD simulation trajectory length by extracting their structural and dynamic information into simpler stochastic models and the simulating stochastic trajectories until the spectrum converges: (1) building a single, effective orientational potential-energy function and a local rotational diffusion tensor to simulate hindered Brownian diffusion (HBD method, red)[17,37] and (2) projecting the relevant spin-label coordinates onto a hidden Markov state model to simulate stochastic jump trajectories (HMM method, blue).[34,36] Although these methods were successfully applied to separate sets of experimental data, they have not been directly compared on a common system. Therefore, their relative merits are unclear. Here, we determine which approximate method most accurately models the behavior of the (more accurate) direct method and best agrees with experimental data. As a benchmark compared to previous work, we investigate the spin-labeled amino acid R1[42,43] ((1-oxyl-2,2,5,5-tetramethyl-3-pyrroline-3-methyl) methanethiosulfonate reacted with a cysteine side chain). We deploy the HBD model in its full generality, utilizing a three-angle orientational potential and several recently published methods for calculating the rotational diffusion tensor from MD trajectories. Also, we for the first time investigate the motional dynamics of the spin-labeled amino acid 2,2,6,6-tetramethylpiperidine-1-oxyl-4-amino-4-carboxylic acid (TOAC),[44−48] provide a force field parameterization, and identify a HMM-based motional model with up to four states that reproduces the MD dynamics very well.

A secondary aim of this paper is to provide a consolidated, modular approach to the time-domain EPR spectral simulation problem. There are many relevant works that use various formalisms and strategies (see refs 19, 29 for comprehensive reviews). However, there has not been a comprehensive software that takes advantage of the best aspects of each approach and allows direct comparisons. Here we present a single, unified framework newly implemented in EasySpin,[13] a freely available software suite in MATLAB.

The structure of this paper is as follows. We first present the theory of time-domain EPR spectral simulations. We describe how the approximate HBD and HMM models are constructed from the MD trajectories and how they are used to generate stochastic trajectories and simulate EPR spectra. Then, we compare the results of the HBD and HMM methods with the direct method. We first examine two model systems: a simple helical peptide (a 20-residue polyalanine helix) labeled with the spin labels R1 and TOAC. Then, we investigate two more realistic systems: the globular soluble protein T4 lysozyme labeled with R1 and the membrane protein phospholamban labeled with TOAC. For these systems, we also compare the simulated spectra with experimental data.

Despite these comparisons, the main goal of this paper is to compare the direct MD method to the approximate HBD and HMM models and not to provide fully converged MD trajectories. Other works have extensively addressed the problem of undersampling during MD simulations using techniques such as umbrella-sampling[36] and replica-exchange dynamics.[39]

DOI: 10.1021/acs.jpcb.9b02693
J. Phys. Chem. B 2019, 123, 10131−10141

THEORY

In this section, we summarize the theory for the three methods (direct, HBD, and HMM) shown in Figure 1. Additional details are given in the Supporting Information (SI). All of the methods presented here are implemented in EasySpin,[13] thus providing a unified platform for consistent model evaluation and comparison.

Orientational and Dihedral Trajectories. Starting from a given MD trajectory, first the global motion of the protein is removed, using a standard method that is spelled out in the SI. This yields an MD trajectory that only contains internal motions. From this, two reduced trajectories are calculated: the orientational trajectory of a spin-label-fixed frame M, needed in all three methods, and a trajectory of spin-label side-chain dihedral angles, needed for the HMM model.

The definition of frame M for both nitroxides (R1 and TOAC) is shown in Figure 2. Letting $\mathbf{O}$, $\mathbf{C}_1$, and $\mathbf{C}_2$ represent

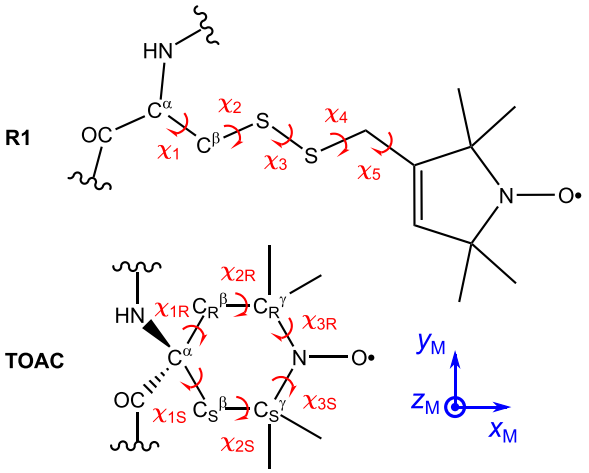

Figure 2. Spin labels R1 and TOAC. The molecular frame, valid for both labels and defined in eq 1, is shown in blue on the lower right. The side-chain dihedral angles are shown in red.

the vectors from the nitrogen atom to the adjacent oxygen and carbon atoms, the frame vectors are[20]

$$\boldsymbol{x}_M = \frac{\boldsymbol{o}}{\|\boldsymbol{o}\|}; \quad \boldsymbol{z}_M = \frac{\mathbf{C}_2\times\boldsymbol{o}+\boldsymbol{o}\times\mathbf{C}_1}{\|\mathbf{C}_2\times\boldsymbol{o}+\boldsymbol{o}\times\mathbf{C}_1\|}; \quad \boldsymbol{y}_M = \boldsymbol{z}_M\times\boldsymbol{x}_M \tag{1}$$

These vectors are combined into a rotation matrix $\boldsymbol{R} = (\boldsymbol{x}_M, \boldsymbol{y}_M, \boldsymbol{z}_M)$. The matrix $\boldsymbol{R}$ is calculated for each time point in the MD trajectory. The time sequence of $\boldsymbol{R}(t)$ constitutes one representation of the orientational trajectory $\boldsymbol{\Omega}(t)$. Alternative representations are obtained by converting the rotation matrices to quaternions, Euler angle triplets, or Wigner D-matrices, as needed. Further details on this are given in the SI.

The angles for the dihedral trajectory are defined as shown in Figure 2. For R1, we use the five side-chain dihedral angles, $\boldsymbol{\chi} = (\chi_1, \chi_2, \chi_3, \chi_4, \chi_5)$. For TOAC, two of its six dihedral angles are sufficient to describe its side-chain conformation. We use $\boldsymbol{\chi} = (\chi_{S2}, \chi_{R2})$ with the endocyclic torsion angles $\chi_{S2} = C^\alpha - C_S^\beta - C_S^\gamma - N^\delta$ and $\chi_{R2} = C^\alpha - C_R^\beta - C_R^\gamma - N^\delta$. R and S indicate pro-R and pro-S relative to the prochiral C^α. The time sequence of $\boldsymbol{\chi}(t)$ constitutes the dihedral trajectory.

HBD Model. For the MD-based HBD method and for modeling global rotational diffusion for combining with local dynamics, we utilize single-particle hindered Brownian rotational diffusion (HBD) dynamics. Implementation and notation for this commonly applied model vary across previous works.[17,20,24,33,37,40,41,49−51] The implementation given here is based on refs 17, 18, 20, 33. Full details are given in the SI.

Briefly, we generate stochastic trajectories by integrating the noninertial Euler−Langevin equation for the angular velocity, using a quaternion representation for the orientation. This stochastic equation depends on the orientational gradient $\nabla V(\boldsymbol{\Omega})$ of an effective orientational potential energy $V(\boldsymbol{\Omega})$ and on an anisotropic spin-label-fixed local rotational diffusion tensor $\boldsymbol{D}_{\text{local}}$. Numerical integration of this equation, starting from given initial orientations, yields stochastic orientational trajectories.

We obtain $V(\boldsymbol{\Omega})$ from the MD-derived orientational trajectories. For this, we first construct the numerical histogram over Euler angles of all orientations occurring in the orientational trajectories. We use a grid with 4° resolution for each of the three Euler angles and apply a convolutional Gaussian smoothing filter with a standard deviation of 2.6°. If built from sufficiently long trajectories, the histogram approximates the equilibrium orientational probability distribution, $P_{\text{eq}}(\boldsymbol{\Omega})$. The potential-energy histogram is then obtained via

$$V(\boldsymbol{\Omega}) = -k_B T \ln P_{\text{eq}}(\boldsymbol{\Omega}) \tag{2}$$

From this, $\nabla V(\boldsymbol{\Omega})$ is calculated numerically and then represented as a gridded interpolant for use in repeated sampling. As an alternative, EasySpin also supports using a complete Wigner function expansion model for $V(\boldsymbol{\Omega})$ with an analytical gradient when simulating stochastic orientational trajectories. For details, see the SI.

To extract an effective rotational diffusion tensor $\boldsymbol{D}_{\text{local}}$ from an MD trajectory, known techniques from recent literature are based on short-time least-squares fitting of the mean square angular displacement (MSAD),[52] autocorrelation functions of quaternion rotations,[53] or fitting of quaternion covariance functions over the entire trajectory,[54] though only for unrestricted rotational diffusion. Here, we apply the MSAD method, though we apply it to the quaternions obtained from the spin-label orientational trajectory and not to those obtained from minimizing the atomic root-mean-square deviation (RMSD) between snapshots (see the SI for details). Previous work on MD-based EPR simulations disregarded the dynamic information contained in the MD trajectories and used a diffusion tensor only as a fitting parameter when modeling experimental data.[17,18,37]

Finally, the resulting stochastic orientational trajectories are converted to interaction tensor trajectories.

HMM Model. The MD-based hidden Markov model (HMM) with multivariate Gaussian emission probabilities is built in several steps.[34,55]

For R1, if the trajectory does not have enough transitions between the two sets of conformations with $\chi_3 \approx \pm 90°$, the longest subtrajectory in one χ_3 state is extracted. We consider a transition undersampled if it occurs less than about 20 times during a microsecond-long MD trajectory. Similarly, if TOAC transitions are undersampled, we extract the longest subtrajectory from one of the sufficiently sampled conformational subspaces.

Next, we categorize the snapshots from the $\boldsymbol{\chi}$ trajectory into N clusters based on their conformational similarity using k-means clustering. The choice of N is described below. The Euclidean distance metric between two $\boldsymbol{\chi}$ vectors needs to

DOI: 10.1021/acs.jpcb.9b02693
J. Phys. Chem. B 2019, 123, 10131−10141

carefully take into account the circular nature of the angles. The cluster centroids are initialized by choosing random points from the time series using the k-means++ algorithm.[56] This process is performed at least 10 times using different initializations, and the best result is selected. The cluster analysis assigns each snapshot to one of the N clusters, resulting in a hidden-state jump trajectory. Additionally, it yields a set of centroids $\{\tilde{\boldsymbol{\mu}}_k\}$ and covariance matrices $\{\tilde{\boldsymbol{\Sigma}}_k\}$ of multivariate Gaussian distributions summarizing the location and spread of each of the N clusters in the dihedral space.

In the next step, the $\boldsymbol{\chi}$ and state trajectories are downsampled to a desired lag time τ_{lag} of the HMM, usually on the order of 100 ps (more on how τ_{lag} is chosen later). From the state trajectories, a transition probability matrix $\tilde{\boldsymbol{P}}$ and stationary probability distribution $\tilde{\boldsymbol{\pi}}$ are calculated while enforcing detailed balance using the L-BFGS algorithm.[57,58] Finally, an initial population distribution $\tilde{\boldsymbol{p}}$ is initialized using $\tilde{\boldsymbol{\pi}}$.

Together, the parameters $(\{\tilde{\boldsymbol{\mu}}_k\}, \{\tilde{\boldsymbol{\Sigma}}_k\}, \tilde{\boldsymbol{p}}, \tilde{\boldsymbol{P}})$ constitute the first guess of the parameters of the HMM model. They are then refined using the expectation−maximization algorithm,[59−61] yielding the optimized HMM model parameters $(\{\boldsymbol{\mu}_k\}, \{\boldsymbol{\Sigma}_k\}, \boldsymbol{p}, \boldsymbol{P})$, where detailed balance is again enforced at every step. For this model, the most-probable state trajectory associated with the downsampled, MD-derived $\boldsymbol{\chi}$ trajectory is calculated using the Viterbi algorithm.[61] Occasionally, states are missing from this state trajectory due to low probabilities, which can be caused by undersampling or using too many states in the HMM construction. In such cases, the entries for nonsampled hidden states are removed from $(\{\boldsymbol{\mu}_k\}, \{\boldsymbol{\Sigma}_k\}, \boldsymbol{p})$, and $(\boldsymbol{P}, \boldsymbol{\pi})$ are recalculated.

The choice of N for the HMM is important. For R1-labeled proteins, N = 54 states are used in the cluster analysis to accommodate the expected multiplicity of energy minima along χ_1 (3), χ_2 (3), χ_4 (3), and χ_5 (2) when in either of the $\chi_3 \approx \pm 90°$ states (the latter are designated here as p_3 and m_3, respectively). The transition rate between p_3 and m_3 states is very slow compared to the length of typical MD simulation trajectories,[34,39] making it prone to undersampling. However, it is also very slow on the EPR time scale at X-band and higher frequencies. Therefore, the two χ_3 subpopulations are treated as isolated dynamic ensembles. Here, we use a p_3 state as a starting conformation for the MD trajectories and use the longest portions of MD trajectories during which R1 remained in p_3 states. Results obtained from m_3 are given in the SI. For TOAC-labeled proteins, we use N = 4 and 2 states for TOAC-polyalanine and TOAC-phospholamban, respectively, to account for twist-boat and chair conformations of the six-membered ring that are observed in the MD trajectories. We indicate the four possible conformers as mm, pm, mp, and pp, according to the signs of χ_{S2} and χ_{R2}. As with the slow transition rates between p_3/m_3 for R1, for TOAC-polyalanine transition rates are slow between the twist-boat state mm and the other chair (mp and pm) and twist-boat (pp) conformations, so a CW EPR spectrum was simulated using the longest portion of MD trajectory belonging to the latter subpopulation.

The second important HMM parameter that must be chosen is the lag time τ_{lag}. The conformational coordinates $\boldsymbol{\chi}$ must be sampled from MD trajectories at a time lag τ_{lag} such that the resulting time series is approximately Markovian (memoryless). However, at the time scale between MD-trajectory snapshots, typically around 1 ps, the dynamics is strongly inertial, and the spin-label dynamics is coupled to nearby conformational degrees of freedom. Therefore, τ_{lag} values much larger than that are required. To identify an appropriate value for τ_{lag}, the relaxation time scales τ_i are examined. These are calculated from the left eigenvalues λ_i of $\boldsymbol{P}$

$$\tau_i = -\tau_{\text{lag}}/\ln \lambda_i \tag{3}$$

Regions of τ_{lag} where all τ_i are approximately independent of τ_{lag} indicate that the associated state trajectories are approximately Markovian. Additionally, τ_{lag} should be chosen to be larger than all τ_i, to assure proper representation of the associated dynamics.

From the N-state HMM model, we generate a number of state jump trajectories (Markov chains) of sufficient length. For each trajectory, first a stochastic initial state is generated by sampling from the equilibrium distribution $\boldsymbol{\pi}$. States at subsequent time points are generated by sampling from the conditional probability distributions, i.e., the rows of the transition probability matrix $\boldsymbol{P}$. Details about the sampling algorithm are given in the SI.

The resulting state trajectories are converted to trajectories of interaction tensors utilizing state-specific effective tensors. These are calculated for each state k of the N states by averaging tensors over all MD frames assigned to a given state k.

Trajectory Processing. The time step used in the spatial trajectories, both MD and stochastic, can be quite small (1 ps $< \Delta t <$ 100 ps). However, since EPR spectra at X-band are not very sensitive to changes in dynamics at those time scales and because propagation of the quantum dynamics is computationally expensive, we employ time-block averaging of the interaction tensors[20] to coarse grain the time step to a larger value. The time step must satisfy the Nyquist criterion $\Delta t < 1/(2\Delta\nu)$, where $\Delta\nu$ is the frequency bandwidth of the spectrum. For a ^{14}N nitroxide at X-band, $1/(2\Delta\nu)$ is about 2.2 ns.

In addition, for the direct method, a "sliding time window" technique[20,26,28,33] was employed to most efficiently utilize the information contained in the long MD trajectories. This method generates multiple shorter trajectories from a long tensor trajectory. More details are given in the SI.

Finally, molecular diffusion rates are known to be underestimated in MD simulations employing the TIP3P water model.[62,63] As such, based on previous MD-based EPR spectral simulation works,[33,35,36] the time step of the spatial trajectories was scaled as needed to correspondingly correct the diffusion rates of the spin label due to its degree of water exposure. These scaling factors are given explicitly in the Results section.

Quantum Spin Propagation. The tensor trajectories, obtained either from the MD-based orientational trajectories or from the HBD- and HMM-based stochastic trajectories, are used for time evolution of the spin-space density operator $\hat{\rho}(t)$ based on the Liouville−von Neumann (LvN) equation

$$\frac{\mathrm{d}}{\mathrm{d}t}\hat{\rho}(t) = -\mathrm{i}\,[\hat{H}(t), \hat{\rho}(t)] \tag{4}$$

The experiment that is simulated is a simple pulse−acquire with a 90° pulse, resulting in an FID

$$M_+(t) \propto \langle \hat{S}_+ \hat{\rho}(t) \rangle \tag{5}$$

where the angled brackets indicate an ensemble average over all trajectories (see Figure 3). The number of trajectories must be chosen such that the overall FID is converged.

DOI: 10.1021/acs.jpcb.9b02693
J. Phys. Chem. B 2019, 123, 10131−10141

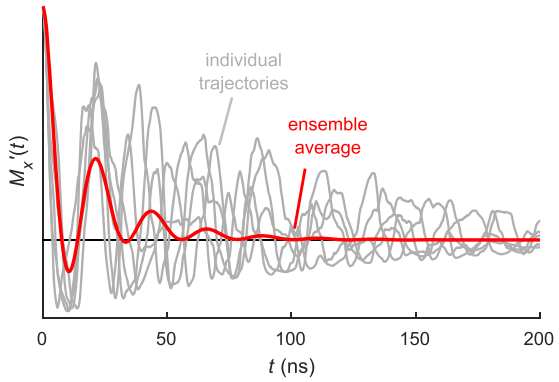

Figure 3. In-phase part of FID signals of an ^{14}N nitroxide simulated from five individual stochastic trajectories with the same starting orientation (gray) and an ensemble average over 80 000 trajectories (red). Each trajectory was simulated using isotropic Brownian rotational diffusion with a diffusion constant D = 0.11 rad^2 ns^{-1} (rotational correlation time τ_R = 1.5 ns) and additional Lorentzian broadening of 0.1 mT ($T_2 \approx$ 110 ns).

To integrate the LvN equation, we implement two methods that differ in scope and performance. One represents the spin Hamiltonian in terms of irreducible spherical tensor operators and is applicable to spin systems with any number of spins of arbitrary multiplicity.[28,41,64,65] The second approach specializes the Hamiltonian and the above equations to the case of S = 1/2 with up to one nucleus, neglecting nuclear Zeeman and nuclear quadrupole interactions as well as nonsecular components of the hyperfine interaction.[20,33] Both approaches yield identical results for nitroxides. However, since the second approach is significantly faster, we utilize it for the nitroxide simulations in this paper. Full details about both approaches are provided in the SI.

The converged FID is then used to calculate the frequency-swept CW EPR absorption spectrum $I(\omega)$ via Fourier transformation

$$I(\omega) \propto \mathrm{Re}\left(\int_0^\infty \mathrm{d}t\ \mathrm{e}^{-\mathrm{i}\omega t} M_+(t)\right) \tag{6}$$

The field-swept CW EPR spectrum is obtained from $I(\omega)$ by converting the frequency axis to a field axis. The first-harmonic CW EPR spectrum is obtained by numerical differentiation, by pseudomodulation, or by multiplication with $2\pi\,\mathrm{i}\,t$ prior to Fourier transformation.

Since this paper focuses on the effects of MD-based models on CW EPR spectral lineshapes, spin relaxation mechanisms other than those due to rotational diffusion are not explicitly treated. Additional homogeneous and inhomogeneous broadening mechanisms that commonly affect CW EPR spectra[66,67] are treated phenomenologically using spectral convolution.

RESULTS AND DISCUSSION

In this section, we compare the results of simulating CW EPR spectra from MD simulations using the approximate HBD and HMM methods against those of the direct method and, when applicable, experimental data. We examine four MD-simulated spin-labeled protein systems: a simple helical peptide (R1-polyalanine and TOAC-polyalanine), a water-soluble protein (R1-T4 lysozyme), and a membrane protein (TOAC-phospholamban). The EPR spectral simulation parameters corresponding to each model are shown in Table 1 (additional parameters are given in the SI). The molecular modeling and rendering for figures was performed using VMD.[68] All EPR spectra in the main text were simulated using an X-band frequency (9.5 GHz); additional spectra simulated using a W-band frequency (95 GHz) are given in the SI.

Table 1. List of EPR Spectral Simulation Parameters for Each Model

model	g	$A/2\pi$ (MHz)	D_{global} (rad^2 μs^{-1})[c]
R1-polyalanine	[2.00900 2.00600 2.00200]	[16.8 16.8 100.9]	0
TOAC-polyalanine	[2.00900 2.00600 2.00200]	[16.8 16.8 100.9]	0
R1-T4 lysozyme[a]	[2.00811 2.00586 2.00202]	[16.8 11.2 103.7]	18
TOAC-phospholamban[b]	[2.00861 2.00622 2.00205]	[16.3 11.2 93.3]	0

[a]From ref 36. [b]Determined by nonlinear least-squares fitting to the direct result. [c]Diffusion rate used to superimpose trajectories of isotropic global rotational diffusion.

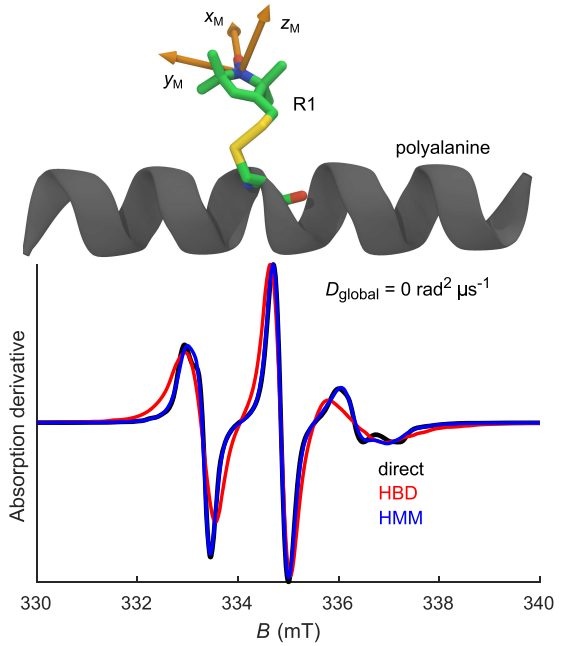

Figure 4. (Top) Snapshot of R1-labeled polyalanine taken from an 800 ns MD simulation trajectory. The molecule-fixed coordinate system that was used to extract the orientation of the spin label's Zeeman and hyperfine interaction tensors is indicated in orange (x-, y-, and z-axes). (Bottom) Corresponding CW EPR spectra simulated based on the MD simulation trajectory with state p_3 using the direct (black), HBD (red), and HMM (blue) methods.

In an effort to more efficiently sample the conformational space of R1, some previous works[33−36] simulated many short MD trajectories (10−100 ns long each) with different starting conformations of R1. Other works[28,30−32,39] have employed single MD trajectories of varying length when simulating CW EPR spectra with some success. Here, for each spin-labeled protein, we simulated one long MD trajectory (800 ns to 1 μs) with spin label starting conformations chosen by energy minimization. This strategy was adopted to assess the efficacy of each spectral simulation method when given a minimal set of MD-trajectory data and provide a valid comparison between the direct method and the others. Although the HBD and

DOI: 10.1021/acs.jpcb.9b02693
J. Phys. Chem. B 2019, 123, 10131−10141

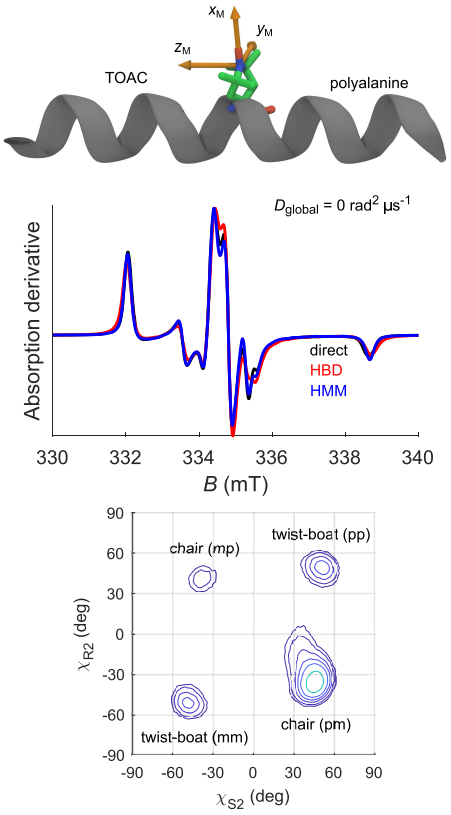

Figure 5. (Top) Snapshot of TOAC-labeled polyalanine taken from a 1 μs MD trajectory. (Center) Corresponding CW EPR spectra simulated based on the MD trajectory with states mp, pm, and pp using the direct (black), HBD (red), and HMM (blue) methods. (Bottom) Histogram of the distribution of TOAC endocyclic torsion angles in the MD trajectory, using contour levels at 1, 2, 5, 10, 20, and 50% of the maximum value.

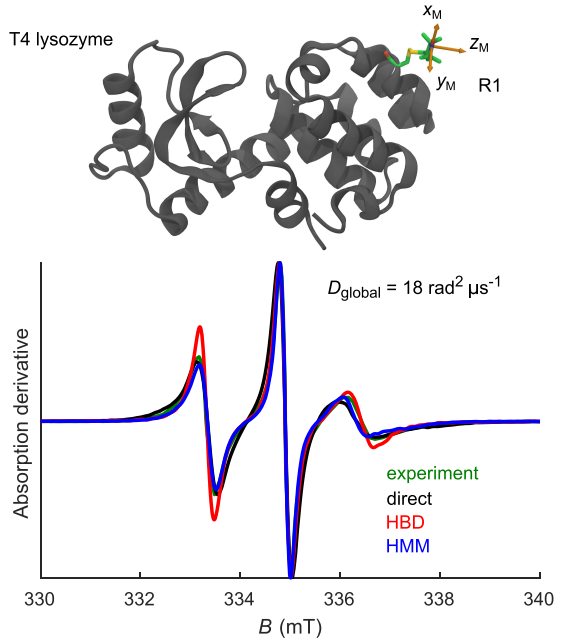

Figure 6. (Top) Snapshot of V131R1-labeled T4 lysozyme taken from an MD trajectory. (Bottom) Experimental (green) and simulated CW EPR spectra. The simulated spectra are based on the MD trajectory with p_3 using the direct (black), HBD (red), and HMM (blue) methods with D_{global} = 18 rad^2 μs^{-1}. The experimental data was taken from ref 77.

HMM methods are capable of utilizing multiple short MD trajectories with T < 100 ns, the minimum required trajectory length for the direct method is the decay time of the FID, on the order of 100−200 ns at X-band and 30−80 ns at W-band.

As a result, transitions that are very slow on the X-band CW EPR time scale, such as those between p_3/m_3 for R1 and p_{2R}/m_{2R} for TOAC, are indeed undersampled in the MD-trajectory data. However, the contribution of such long-lived states toward the total CW EPR spectrum can be approximated by simulating spectra from each of these states individually and adding them linearly. For these reasons and to avoid undersampling transitions, when simulating CW EPR spectra, we selected the longest portions of each trajectory during which the spin label remained in these long-lived states. We consider a given dihedral state undersampled if the total number of transitions into and out of it is less than about 20. Although such cases could accurately reflect a transition rate on the time scale of the MD-trajectory length, the associated large uncertainty will significantly affect their estimation. Regarding convergence behavior of the spectral simulation methods, in the SI we examine the effects of varying the MD-trajectory length used to simulate each spectrum.

For each MD simulation, the integration time step was 2 fs and the time step between saving snapshots was 2 ps. More detailed information regarding the MD and spectral simulations as well as the trajectories of the dihedral angles χ for each spin-labeled system can be found in the SI.

R1- and TOAC-Polyalanine. As simple model systems, following the example set by ref 33, we use two water-solvated 20-residue polyalanine helices, labeled with either R1 (attached to a cysteine) or TOAC (mutated from alanine) at position 10. To prevent unfolding of the helix in the all-atom MD simulations, the backbone atoms of the helix were harmonically restrained in each case. The time axis was scaled by a factor of 2.5 due to the labeling site's high water exposure, as was done in refs 33, 35. Cartoons of the spin-label/helix systems, excluding solvent molecules, are shown at the top of Figures 4 and 5, along with the molecule-fixed frames.

No global diffusion was superimposed so as to examine the effects of spin-label motion on CW EPR spectra in the absence of peptide tumbling. There exist experimental data of spin-labeled peptides tumbling in the solution for both R1[69−72] and TOAC.[73,74] However, in these data, the spin-label motion is masked by the rapid and anisotropic nature of the peptide's global motion. There do not appear to be experimental data in which the spin-label motion is unhindered and the peptide is immobilized. As a result, the approximate method results are compared with those of the direct method in this section.

The CW EPR spectra simulated from the MD trajectory of R1-polyalanine using the direct (black), HBD (red), and HMM (blue) methods are shown at the bottom of Figure 4. The direct method result shows a relatively sharp lineshape indicating fast reorientational motion with a correlation time on the order of sub-nanoseconds. The high- and low-field lines each show two distinct features, which are probably caused by differential degrees of motional restriction between rotameric states of the label. These features are only captured by the HMM method. In the HBD method, the orientational histogram has several prominent maxima, and $\boldsymbol{D}_{local} \approx$ (208, 280, 630) rad^2 μs^{-1} (we represent $\boldsymbol{D}_{local}$ using its eigenvalues here and throughout this section) was obtained from fitting the

DOI: 10.1021/acs.jpcb.9b02693
J. Phys. Chem. B 2019, 123, 10131−10141

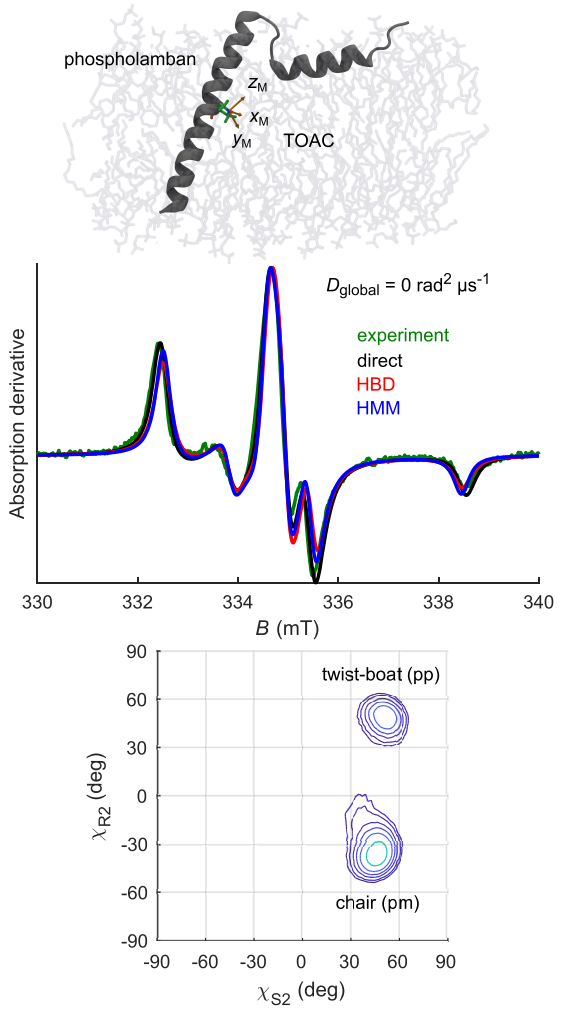

Figure 7. (Top) Snapshot of TOAC-labeled phospholamban in a lipid bilayer taken from an MD trajectory. (Center) Corresponding CW EPR spectra from the experiment (green) and simulation based on the MD trajectory using the direct (black), HBD (red), and HMM (blue) methods. (Bottom) Histogram of the distribution of TOAC endocyclic torsion angles in the MD trajectory, using contour levels at 1, 2, 5, 10, 20, and 50% of the maximum value.

MSAD of the label's orientational trajectory. However, the HBD spectrum is significantly more broadened than that of the direct method, indicating that the time scales of the estimated rotational diffusion tensor are too slow. On the other hand, the HMM method result agrees significantly better with the direct method, although the features are slightly more broadened. This could be due to faster transition rates between states or lesser differences in motional restriction. For additional simulated CW EPR spectra of R1-labeled polyalanine using a different starting conformation (m_3), see the SI.

For TOAC-labeled polyalanine (Figure 5), the simulated EPR spectra reflect reorientational motion near the rigid limit. The dynamics of TOAC here more closely resembles multisite exchange among four states (two twist-boat and two chair ring conformations) rather than Brownian rotational diffusion. State lifetimes differed greatly. For example, the chair conformation $\chi \approx (44, -33°)$ has a lifetime of 3.0 ns, whereas $\chi \approx (-38, 40°)$ has a lifetime of 0.3 ns, as determined by the HMM method. The HBD method showed several prominent, sharp maxima as the only features shown in the orientational histogram, and $\boldsymbol{D}_{local} \approx (44, 79, 35)$ rad^2 μs^{-1}, indicating that TOAC is undergoing fast, very restricted dynamics. This model provides a reasonable approximation of the direct-method spectrum, though the HBD lineshape is consistently broader. The spectrum from the HMM method, on the other hand, is nearly identical to that of the direct method, thus validating the four-state ring conformation model of TOAC's dynamics. This is because the HMM is capable of approximating stochastic jump behavior with multiple time scales between orientationally averaged states.

R1-T4 Lysozyme. The first realistic MD-simulated system is water-solvated R1-labeled V131C T4 lysozyme[75] (PDB ID 5G27, where existing ligands were removed). In this case, the entire label-protein system was allowed to undergo unrestrained dynamics for a single 1 μs trajectory. To avoid biases due to undersampling of global protein tumbling, the global motion was removed from the MD trajectory by least-squares atomic RMSD alignment of the protein between snapshots (see the SI). Based on an estimate obtained from fitting experimental CW EPR spectra of T4 lysozyme in an earlier work,[76] stochastic global rotational diffusion with D_{global} = 18 rad^2 μs^{-1} was then superimposed on the MD-derived orientational trajectories. Additionally, the time axis for this model was scaled by a factor of 2.0,[36] as the solvent exposure was expected to be slightly less than R1-labeled polyalanine.

Figure 6 shows the simulated CW EPR spectra for V131R1 T4 lysozyme. The experimental spectrum (green) reflects reorientational motion with a correlation time on the order of nanoseconds with some orientational ordering. This is expected for a solvent-exposed labeling site located on a short helix that would provide motional ordering. The direct result (black) agrees relatively well with the experimental result. The HBD method result (red) was obtained using $\boldsymbol{D}_{local}$ = (220, 220, 340) rad^2 μs^{-1} as extracted from the MD trajectory, and the orientational histogram showed a large number of peaks. Compared to the experiment, the HBD spectrum shows sharper features, indicating that the HBD model is faster and/or less orientationally restricted. In contrast, the HMM simulation agrees excellently with the experiment. The results show that a majority of the state lifetimes are less than 1 ns. See the SI for additional simulated CW EPR spectra of R1-labeled T4 lysozyme with a different starting conformation (m_3). The HBD method showed better agreement with the experiment for this other starting conformation, indicating different effective types of orientational motion between the two conformational subspaces.

TOAC-Phospholamban. We also simulated CW EPR spectra based on a 1 μs long MD simulation of TOAC-labeled phospholamban[78] (at position 37 of PDB ID 2KB7) in a lipid bilayer. In contrast to TOAC-polyalanine, here only two ring puckering states were revealed (one twist-boat and one chair conformation) and were used for the HMM method. The smaller number of TOAC conformer states compared to TOAC-polyalanine is probably due to steric effects, such as the presence of the bulky neighboring F36 and L38 sidechains in phospholamban compared to the smaller alanine neighbors in polyalanine. Unlike for the peptide and T4L, the time axis was not scaled since the spin-label location is buried inside the lipid bilayer, and the incorrect viscosity of TIP3P water will not affect the spin-label dynamics. The global motion of phospholamban was not removed for the spectral simulations in this section, as including it yielded excellent agreement with the experiment.

DOI: 10.1021/acs.jpcb.9b02693
J. Phys. Chem. B 2019, 123, 10131−10141

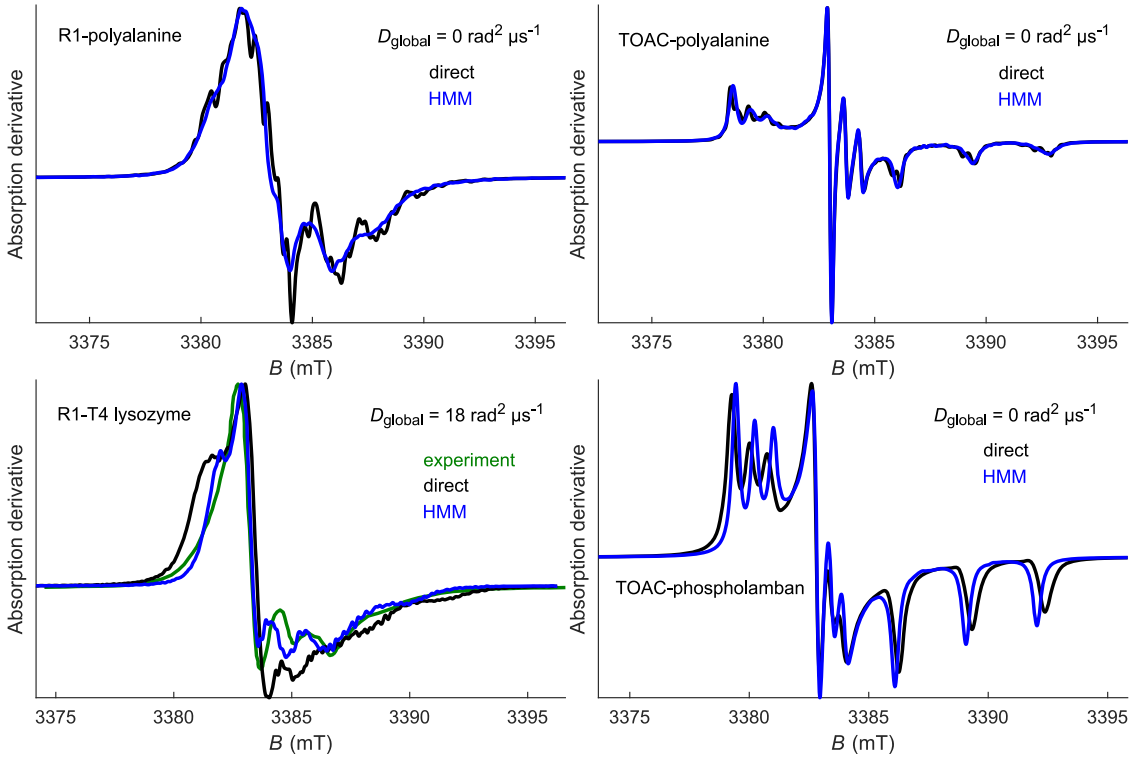

Figure 8. W-band EPR spectra (95 GHz) simulated using the direct (black) and HMM (blue) methods. Experimental data only available for R1-labeled T4 lysozyme (green) is from ref 77.

Figure 7 shows the directly simulated CW EPR spectrum (black) together with the HBD simulation (red), the HMM simulation (blue), and the experimental spectrum (green). As expected for the conformationally restricted TOAC label located on a transmembrane helix, the experimental spectrum shows a lineshape of reorientational motion that is very slow on the time scale of X-band EPR. Once again, the direct method showed excellent agreement with the experiment, indicating that TOAC's conformational dynamics was sufficiently sampled by the MD trajectory. Regarding the HBD method result, as with TOAC-polyalanine, the principal values of the fitted rotational diffusion tensor ($\boldsymbol{D}_{local}$ = (10, 13, 7) rad^2 μs^{-1}) were large. This showed relatively good agreement with the experiment, further confirming that the optimal Brownian model for approximating TOAC's behavior is fast, very restricted dynamics. The improved HBD method agreement here relative to TOAC-polyalanine is probably due to the greater conformational restriction exhibited for TOAC-phospholamban (two states vs. four states), making the effects of multisite exchange with multiple transition time scales less significant. Finally, the HMM method showed excellent agreement as well, which further validates the strategy of using TOAC's ring puckering to model its reorientational dynamics.

W-Band EPR Spectra. To complement the X-band EPR spectra simulated and discussed above, we also simulated W-band spectra for each model using the direct and HMM methods. Experimentally, a multifrequency analysis provides stronger constraints on dynamic parameters that are extractable from the data. Additionally, spectra acquired at W-band frequencies are more sensitive to faster dynamics relative to X-band, allowing one to more closely examine the effects of spin-label side-chain dynamics. We did not include the HBD method here, as it performs worse than HMM already at X-band.

The W-band simulations are shown in Figure 8. Confirming the results shown by X-band spectra, the W-band spectra show that the HMM is able to reasonably approximate the result of the direct simulation. The agreement is excellent for TOAC-polyalanine. For R1-polyalanine, the choppiness of the direct-method spectrum is due to the longest subtrajectory within the p_3 conformational subspace being too short (ca. 600 ns) to fully sample R1 dynamics, whereas for the HMM simulation, as many stochastic trajectories can be simulated as needed to converge the simulated spectrum. Note that both spectra are simulated without additional global rotational diffusion. Adding global rotational diffusion renders the agreement between the two excellent, as shown in the SI.

There are discrepancies between the direct and HMM methods for R1-T4 lysozyme and TOAC-phospholamban. By comparing with the X-band spectra counterparts, the differences that are already present in the X-band spectra are now enhanced in the W-band spectra. For R1-T4 lysozyme, the direct-method spectrum shows a larger degree of broadening. For TOAC-phospholamban, the direct-method spectrum is wider as well. Both indicate slower apparent dynamics for the direct method in their respective motional regimes (slow vs. very slow). Finally, the comparison between HMM simulation and experiment reveals an agreement similar to that shown in ref 36, further confirming that the HMM parameters are well determined from the MD trajectory.

■ CONCLUSIONS

In this paper, several trajectory-based time-domain methods of CW EPR spectral simulation based on MD simulations of spin-labeled proteins were presented. Three models of MD-derived

DOI: 10.1021/acs.jpcb.9b02693
J. Phys. Chem. B 2019, 123, 10131−10141

spin-label dynamics of differing complexity (direct MD, HBD, and HMM) were examined and compared across three different proteins and two spin labels with very different mobilities: R1 and TOAC.

When compared with experimental data, the direct method worked very well for both slow motion in TOAC-phospholamban and faster motion in R1-T4 lysozyme, indicating sufficient conformational sampling in each MD trajectory. In general, more advanced sampling methods such as umbrella-sampling[36] and replica-exchange dynamics[39] will be needed to ascertain complete sampling.

Regarding the approximate methods (HBD and HMM), the HMM method is, in general, superior as it can account for multiple time scales for transitions between spin-label orientations, whereas the HBD method only uses a single rotational diffusion tensor and an orientational potential energy. Given its stark simplicity, the HBD method performed surprisingly well. However, for the very restricted, multisite jump-like motion of TOAC-polyalanine as well as for both R1-labeled systems, the HMM method was clearly superior compared to the HBD method, indicating the flexibility of the HMM method for spin labels with different types of dynamics. For these reasons and due to its consistent performance, we conclude that the HMM method is the preferred approximation for simulating EPR spectra from MD simulations, both for R1 and TOAC labels.

The computation times for the faster-motion spectra of R1-labeled proteins using HBD were about 50 times longer than with HMM. The bottleneck in the HBD method is the interpolative evaluation of the torque term at each time step. This is a second reason for which the HMM is preferred.

To the authors' knowledge, TOAC-labeled proteins had not been studied via MD simulation prior to this work. The results given here show that the dynamics of TOAC in α-helical sites can be accurately modeled as two- or four-site exchange between twist-boat and chair conformations.

Finally, a key practical aspect of the present work is that all three models of spin-label dynamics as well as the ability to directly interface with MD simulation data have been implemented in a time-domain CW EPR spectral simulation software suite in the freely available software EasySpin.[13] This allows anyone to perform similar spectral simulations using dynamical orientational trajectories from any MD program and test different models of spin-label dynamics of nitroxides or any other spin system on a single platform.

■ ASSOCIATED CONTENT

Supporting Information

The Supporting Information is available free of charge at https://pubs.acs.org/doi/10.1021/acs.jpcb.9b02693.

Conversion formulas between different rotation representations, expressions of the orientational potential using Wigner *D*-matrices and quaternions, MD simulation parameters, details on processing MD simulation results, plots of all dihedral trajectories, validation of time-domain CW EPR spectral simulations against a frequency-domain (SLE) solver, m_3 results for the R1-labeled systems, and mm results for TOAC-polyalanine (PDF)

TOAC force field parameters (ZIP)

■ AUTHOR INFORMATION

Corresponding Authors

*E-mail: ddt@umn.edu (D.D.T.). Phone: (612) 626-0957.
*E-mail: stst@uw.edu (S.S.). Phone: (206) 543-2906.

ORCID

Bengt Svensson: 0000-0003-3932-2376
Stefan Stoll: 0000-0003-4255-9550

Notes

The authors declare no competing financial interest.

■ ACKNOWLEDGMENTS

This work was supported by NIH grants GM27906 (D.D.T.), AR32961 (D.D.T.), AG026160 (D.D.T.), and GM125753 (S.S.) and by NSF grant CHE-1452967 (S.S.). P.D.M. was supported by NIH Training Grant AR007612. Computational resources for MD simulations were provided by the Minnesota Supercomputing Institute. We thank Jack H. Freed (Cornell) for providing the CW EPR experimental data for V131R1 T4 lysozyme. We also thank Andrew Reid for performing the MD simulation on TOAC-labeled phospholamban.

■ REFERENCES

(1) Oh, K. J.; Altenbach, C.; Collier, R. J.; Hubbell, W. L. *Site-Directed Spin Labeling of Proteins: Applications to Diphtheria Toxin*; Springer, 2000; Vol. *145*, pp 147−169.

(2) Klug, C. S.; Feix, J. B. Biophysical Tools for Biologists. In *Methods in Cell Biology*; Academic Press, 2008; Vol. *84*, pp 617−658.

(3) Sillescu, H.; Kivelson, D. Theory of Spin-Lattice Relaxation in Classical Liquids. *J. Chem. Phys.* **1968**, *48*, 3493−3505.

(4) Galloway, N. B.; Dalton, L. R. Approximate methods for the fast computation of EPR and ST-EPR spectra. I. A perturbation approach. *Chem. Phys.* **1978**, *30*, 445−459.

(5) McCalley, R.; Shimshick, E.; McConnell, H. The effect of slow rotational motion on paramagnetic resonance spectra. *Chem. Phys. Lett.* **1972**, *13*, 115−119.

(6) Thomas, D. D.; McConnell, H. M. Calculation of paramagnetic resonance spectra sensitive to very slow rotational motion. *Chem. Phys. Lett.* **1974**, *25*, 470−475.

(7) Freed, J. H.; Bruno, G. V.; Polnaszek, C. F. Electron Spin Resonance Line Shapes and Saturation in the Slow Motional Region. *J. Phys. Chem. A.* **1971**, *75*, 3385−3399.

(8) Freed, J. H. *Spin Labeling: Theory and Applications*; Academic Press, 1976; pp 53−132.

(9) Robinson, B. H.; Dalton, L. R. Anisotropic rotational diffusion studied by passage saturation transfer electron paramagnetic resonance. *J. Chem. Phys.* **1980**, *72*, 1312−1324.

(10) Schneider, D. J.; Freed, J. H. *Spin Labeling: Theory and Applications*; Springer: US, 1989; Vol. *8*, pp 1−76.

(11) Earle, K. A.; Budil, D. E. *Calculating Slow-Motion ESR Spectra of Spin-Labeled Polymers*; Wiley-Blackwell, 2006; pp 53−83.

(12) Budil, D. E.; Lee, S.; Saxena, S.; Freed, J. H. Nonlinear-Least-Squares Analysis of Slow-Motion EPR Spectra in One and Two Dimensions Using a Modified Levenberg-Marquardt Algorithm. *J. Magn. Reson., Ser. A* **1996**, *120*, 155−189.

(13) Stoll, S.; Schweiger, A. EasySpin, a comprehensive software package for spectral simulation and analysis in EPR. *J. Magn. Reson.* **2006**, *178*, 42−55.

(14) Raitsimring, A. M.; Gunanathan, C.; Potapov, A.; Efremenko, I.; Martin, J. M. L.; Milstein, D.; Goldfarb, D. Gd^{3+} complexes as potential spin labels for high field pulsed EPR distance measurements. *J. Am. Chem. Soc.* **2007**, *129*, 14138−14139.

(15) Kuzhelev, A. A.; Trukhin, D. V.; Krumkacheva, O. A.; Strizhakov, R. K.; Rogozhnikova, O. Y.; Troitskaya, T. I.; Fedin, M. V.; Tormyshev, V. M.; Bagryanskaya, E. G. Room-Temperature Electron Spin Relaxation of Triarylmethyl Radicals at the X- and Q-Bands. *J. Phys. Chem. B* **2015**, *119*, 13630−13640.

DOI: 10.1021/acs.jpcb.9b02693
J. Phys. Chem. B 2019, 123, 10131−10141

(16) Cunningham, T. F.; Putterman, M. R.; Desai, A.; Horne, W. S.; Saxena, S. The Double-Histidine Cu^{2+}-binding Motif: a Highly Rigid, Site-Specific Spin Probe for Electron Spin Resonance Distance Measurements. *Angew. Chem., Int. Ed.* **2015**, *54*, 6330−6334.
(17) Beier, C.; Steinhoff, H.-J. A Structure-Based Simulation Approach for Electron Paramagnetic Resonance Spectra Using Molecular and Stochastic Dynamics Simulations. *Biophys. J.* **2006**, *91*, 2647−2664.
(18) Budil, D. E.; Sale, K. L.; Khairy, K. A.; Fajer, P. G. Calculating Slow-Motional Electron Paramagnetic Resonance Spectra from Molecular Dynamics Using a Diffusion Operator Approach. *J. Phys. Chem. A* **2006**, *110*, 3703−3713.
(19) Budil, D. E. CW-EPR Spectral Simulations: Slow-Motion Regime. *Methods Enzymol.* **2015**, *563*, 143−170.
(20) DeSensi, S. C.; Rangel, D. P.; Beth, A. H.; Lybrand, T. P.; Hustedt, E. J. Simulation of Nitroxide Electron Paramagnetic Resonance Spectra from Brownian Trajectories and Molecular Dynamics Simulations. *Biophys. J.* **2008**, *94*, 3798−3809.
(21) Eviatar, H.; van Faassen, E.; Levine, Y. K. A New Approach for the Simulation of ESR Lineshapes Over a Large Range of Correlation Times. *Chem. Phys. Lett.* **1992**, *195*, 233−238.
(22) Eviatar, H.; van Faassen, E. E.; Levine, Y. K.; Hoult, D. I. Time-Domain Simulation of ESR Spectra of Nitroxide Spin Probes. *Chem. Phys.* **1994**, *181*, 369−376.
(23) Håkansson, P.; Westlund, P.; Lindahl, E.; Edholm, O. A Direct Simulation of EPR Slow-Motion Spectra of Spin Labelled Phospholipids in Liquid Crystalline Bilayers Based on a Molecular Dynamics Simulation of the Lipid Dynamics. *Phys. Chem. Chem. Phys.* **2001**, *3*, 5311−5319.
(24) Håkansson, P.; Nair, P. B. Implicit Numerical Schemes for the Stochastic Liouville Equation in Langevin Form. *Phys. Chem. Chem. Phys.* **2011**, *13*, 9578.
(25) Håkansson, P.; Nguyen, T.; Nair, P. B.; Edge, R.; Stulz, E. Cu(II)-porphyrin molecular dynamics as seen in a novel EPR/Stochastic Liouville equation study. *Phys. Chem. Chem. Phys.* **2013**, *15*, 10930−10941.
(26) Oganesyan, V. S. A novel approach to the simulation of nitroxide spin label EPR spectra from a single truncated dynamical trajectory. *J. Magn. Reson.* **2007**, *188*, 196−205.
(27) Oganesyan, V. S.; Kuprusevicius, E.; Gopee, H.; Cammidge, A.; Wilson, M. Electron Paramagnetic Resonance Spectra Simulation Directly from Molecular Dynamics Trajectories of a Liquid Crystal with a Doped Paramagnetic Spin Probe. *Phys. Rev. Lett.* **2009**, *102*, No. 013005.
(28) Oganesyan, V. S. A general approach for prediction of motional EPR spectra from Molecular Dynamics (MD) simulations: application to spin labelled protein. *Phys. Chem. Chem. Phys.* **2011**, *13*, 4724−4737.
(29) Oganesyan, V. S. *Electron Paramagnetic Resonance*; The Royal Society of Chemistry, 2014; Vol. *24*, pp 32−61.
(30) Oganesyan, V. S.; Chami, F.; White, G. F.; Thomson, A. J. A combined EPR and MD simulation study of a nitroxyl spin label with restricted internal mobility sensitive to protein dynamics. *J. Magn. Reson.* **2017**, *274*, 24−35.
(31) Prior, C.; Oganesyan, V. S. Prediction of EPR Spectra of Lyotropic Liquid Crystals using a Combination of Molecular Dynamics Simulations and the Model-Free Approach. *Chem. - Eur. J.* **2017**, *23*, 13192−13204.
(32) Prior, C.; Danīlāne, L.; Oganesyan, V. S. All-atom molecular dynamics simulations of spin labelled double and single-strand DNA for EPR studies. *Phys. Chem. Chem. Phys.* **2018**, *20*, 13461−13472.
(33) Sezer, D.; Freed, J. H.; Roux, B. Simulating electron spin resonance spectra of nitroxide spin labels from molecular dynamics and stochastic trajectories. *J. Chem. Phys.* **2008**, *128*, No. 165106.
(34) Sezer, D.; Freed, J. H.; Roux, B. Using Markov Models to Simulate Electron Spin Resonance Spectra from Molecular Dynamics Trajectories. *J. Phys. Chem. B* **2008**, *112*, 11014−11027.
(35) Sezer, D.; Freed, J. H.; Roux, B. Parametrization, Molecular Dynamics Simulation, and Calculation of Electron Spin Resonance Spectra of a Nitroxide Spin Label on a Polyalanine α-Helix. *J. Phys. Chem. B* **2008**, *112*, 5755−5767.
(36) Sezer, D.; Freed, J. H.; Roux, B. Multifrequency Electron Spin Resonance Spectra of a Spin-Labeled Protein Calculated from Molecular Dynamics Simulations. *J. Am. Chem. Soc.* **2009**, *131*, 2597−2605.
(37) Steinhoff, H. J.; Hubbell, W. L. Calculation of electron paramagnetic resonance spectra from Brownian dynamics trajectories: Application to nitroxide side chains in proteins. *Biophys. J.* **1996**, *71*, 2201−2212.
(38) Stoica, I. Using Molecular Dynamics To Simulate Electronic Spin Resonance Spectra of T4 Lysozyme. *J. Phys. Chem. B* **2004**, *108*, 1771−1782.
(39) Tyrrell, S.; Oganesyan, V. S. Simulation of electron paramagnetic resonance spectra of spin-labeled molecules from replica-exchange molecular dynamics. *Phys. Rev. E* **2013**, *88*, No. 042701.
(40) Usova, N.; Westlund, P.; Fedchenia, I. I. Direct simulation of slowmotion electron spin resonance spectra by solving the stochastic Liouville equation in the time domain with stochastic dynamics in the form of trajectories. *J. Chem. Phys.* **1995**, *103*, 96−103.
(41) Usova, N.; Persson, L.; Westlund, P. Theory of slow-motion EPR lineshapes for studies of membrane curvature. *Phys. Chem. Chem. Phys.* **2000**, *2*, 2785−2793.
(42) Berliner, L. J.; Grunwald, J.; Hankovszky, H.; Hideg, K. A novel reversible thiol-specific spin label: Papain active site labeling and inhibition. *Anal. Biochem.* **1982**, *119*, 450−455.
(43) Mchaourab, H. S.; Lietzow, M. A.; Hideg, K.; Hubbell, W. L. Motion of Spin-Labeled Side Chains in T4 Lysozyme. Correlation with Protein Structure and Dynamics. *Biochemistry* **1996**, *35*, 7692−7704.
(44) Nakaie, C.; Goissis, G.; Schreier, S.; Paiva, A. pH dependence of EPR spectra of nitroxides containing ionizable groups. *Braz. J. Med. Biol. Res.* **1981**, *14*, 173−180.
(45) Toniolo, C.; Valente, E.; Formaggio, F.; Crisma, M.; Pilloni, G.; Corvaja, C.; Toffoletti, A.; Martinez, G. V.; Hanson, M. P.; Millhauser, G. L.; et al. Synthesis and conformational studies of peptides containing TOAC, a spin-labelled Cα,α-disubstituted glycine. *J. Pept. Sci.* **1995**, *1*, 45−57.
(46) D'Amore, M.; Improta, R.; Barone, V. Conformational Behavior and Magnetic Properties of a Nitroxide Amino Acid Derivative in Vacuo and in Aqueous Solution. *J. Phys. Chem. A* **2003**, *107*, 6264−6269.
(47) Marsh, D. Orientation of TOAC amino-acid spin labels in -helices and -strands. *J. Magn. Reson.* **2006**, *180*, 305−310.
(48) Schreier, S.; Bozelli, J. C.; Marn, N.; Vieira, R. F. F.; Nakaie, C. R. The spin label amino acid TOAC and its uses in studies of peptides: chemical, physicochemical, spectroscopic, and conformational aspects. *Biophys. Rev.* **2012**, *4*, 45−66.
(49) Itzkowitz, M. S. Monte Carlo Simulation of the Effects of Molecular Motion on the EPR Spectrum of Nitroxide Free Radicals. *J. Chem. Phys.* **1967**, *46*, 3048−3056.
(50) Robinson, B. H.; Slutsky, L. J.; Auteri, F. P. Direct simulation of continuous wave electron paramagnetic resonance spectra from Brownian dynamics trajectories. *J. Chem. Phys.* **1992**, *96*, 2609−2616.
(51) Rangel, D. P.; Baveye, P. C.; Robinson, B. H. Direct simulation of magnetic resonance relaxation rates and line shapes from molecular trajectories. *J. Phys. Chem. B* **2012**, *116*, 6233−6249.
(52) Chevrot, G.; Hinsen, K.; Kneller, G. R. Model-free simulation approach to molecular diffusion tensors. *J. Chem. Phys.* **2013**, *139*, 154110−154120.
(53) Chen, P.-C.; Hologne, M.; Walker, O. Computing the Rotational Diffusion of Biomolecules via Molecular Dynamics Simulation and Quaternion Orientations. *J. Phys. Chem. B* **2017**, *121*, 1812−1823.
(54) Linke, M.; Köfinger, J.; Hummer, G. Fully Anisotropic Rotational Diffusion Tensor from Molecular Dynamics Simulations. *J. Phys. Chem. B* **2018**, *122*, 5630−5639.
(55) Sezer, D.; Roux, B. Markov state and diffusive stochastic models in electron spin resonance. *Adv. Exp. Med. Biol.* **2014**, *797*, 115−138.

DOI: 10.1021/acs.jpcb.9b02693
J. Phys. Chem. B 2019, 123, 10131−10141

(56) Arthur, D.; Vassilvitskii, S. In *k-means++: The Advantages of Careful Seeding*, Proceedings of the eighteenth annual ACM-SIAM symposium on Discrete algorithms, 2007; pp 1027−1035.
(57) Byrd, R. H.; Lu, P.; Nocedal, J.; Zhu, C. A Limited Memory Algorithm for Bound Constrained Optimization. *SIAM J. Sci. Comput.* **1995**, *16*, 1190−1208.
(58) Becker, S. *L-BFGS-B-C*. https://github.com/stephenbeckr/L-BFGS-B-C, 2019.
(59) Dempster, A. P.; Laird, N. M.; Rubin, D. B. Maximum Likelihood from Incomplete Data via the EM Algorithm. *J. R. Stat. Soc. Ser. B* **1977**, *39*, 1−22.
(60) Liporace, L. Maximum likelihood estimation for multivariate observations of Markov sources. *IEEE Trans. Inf. Theory* **1982**, *28*, 729−734.
(61) Rabiner, L. R. A tutorial on hidden Markov models and selected applications in speech recognition. *Proc. IEEE* **1989**, *77*, 257−286.
(62) Feller, S. E.; Pastor, R. W.; Rojnuckarin, A.; Bogusz, S.; Brooks, B. R. Effect of Electrostatic Force Truncation on Interfacial and Transport Properties of Water. *J. Phys. Chem. A.* **1996**, *100*, 17011−17020.
(63) Yeh, I.-C.; Hummer, G. Diffusion and Electrophoretic Mobility of Single-Stranded RNA from Molecular Dynamics Simulations. *Biophys. J.* **2004**, *86*, 681−689.
(64) Mehring, M. *Principles of High Resolution NMR in Solids*; Springer: Berlin, Heidelberg, 1983.
(65) Liang, Z.; Freed, J. H. An Assessment of the Applicability of Multifrequency ESR to Study the Complex Dynamics of Biomolecules. *J. Phys. Chem. B* **1999**, *103*, 6384−6396.
(66) Robinson, B.; Mailer, C.; Reese, A. Linewidth Analysis of Spin Labels in Liquids: I. Theory and Data Analysis. *J. Magn. Reson.* **1999**, *138*, 199−209.
(67) Robinson, B.; Mailer, C.; Reese, A. Linewidth Analysis of Spin Labels in Liquids: II. Experimental. *J. Magn. Reson.* **1999**, *138*, 210−219.
(68) Humphrey, W.; Dalke, A.; Schulten, K. VMD: Visual Molecular Dynamics. *J. Mol. Graphics* **1996**, *14*, 33−38.
(69) Miick, S. M.; Todd, A. P.; Millhauser, G. L. Position-Dependent Local Motions in Spin-Labeled Analogues of a Short α-Helical Peptide Determined by Electron Spin Resonance. *Biochemistry* **1991**, *30*, 9498−9503.
(70) Todd, A. P.; Millhauser, G. L. ESR Spectra Reflect Local and Global Mobility in a Short Spin-Labeled Peptide throughout the α-Helix Coil Transition. *Biochemistry* **1991**, *30*, 5515−5523.
(71) Miick, S. M.; Casteel, K. M.; Millhauser, G. L. Experimental Molecular Dynamics of an Alanine-Based Helical Peptide Determined by Spin Label Electron Spin Resonance. *Biochemistry* **1993**, *32*, 8014−8021.
(72) Bennati, M.; Gerfen, G. J.; Martinez, G. V.; Griffin, R. G.; Singel, D. J.; Millhauser, G. L. Nitroxide Side-Chain Dynamics in a Spin-Labeled Helix-Forming Peptide Revealed by High-Frequency (139.5-GHz) EPR Spectroscopy. *J. Magn. Reson.* **1999**, *139*, 281−286.
(73) Hanson, P.; Martinez, G.; Millhauser, G.; Formaggio, F.; Crisma, M.; Toniolo, C.; Vita, C. Distinguishing helix conformations in alanine-rich peptides using the unnatural amino acid TOAC and electron spin resonance. *J. Am. Chem. Soc.* **1996**, *118*, 271−272.
(74) McNulty, J. C.; Silapie, J. L.; Carnevali, M.; Farrar, C. T.; Griffin, R. G.; Formaggio, F.; Crisma, M.; Toniolo, C.; Millhauser, G. L. Electron spin resonance of TOAC labeled peptides: Folding transitions and high frequency spectroscopy. *Biopolymers* **2000**, *55*, 479−485.
(75) Consentius, P.; Gohlke, U.; Loll, B.; Alings, C.; Mller, R.; Heinemann, U.; Kaupp, M.; Wahl, M.; Risse, T. Tracking Transient Conformational States of T4 Lysozyme at Room Temperature Combining X-ray Crystallography and Site-Directed Spin Labeling. *J. Am. Chem. Soc.* **2016**, *138*, 12868−12875.
(76) Liang, Z.; Lou, Y.; Freed, J. H.; Columbus, L.; Hubbell, W. L. A Multifrequency Electron Spin Resonance Study of T4 Lysozyme Dynamics Using the Slowly Relaxing Local Structure Model. *J. Phys. Chem. B* **2004**, *108*, 17649−17659.
(77) Zhang, Z.; Fleissner, M. R.; Tipikin, D. S.; Liang, Z.; Moscicki, J. K.; Earle, K. A.; Hubbell, W. L.; Freed, J. H. Multifrequency Electron Spin Resonance Study of the Dynamics of Spin Labeled T4 Lysozyme. *J. Phys. Chem. B* **2010**, *114*, 5503−5521.
(78) Traaseth, N. J.; Shi, L.; Verardi, R.; Mullen, D. G.; Barany, G.; Veglia, G. Structure and topology of monomeric phospholamban in lipid membranes determined by a hybrid solution and solid-state NMR approach. *Proc. Natl. Acad. Sci. U.S.A.* **2009**, *106*, 10165−10170.

DOI: 10.1021/acs.jpcb.9b02693
J. Phys. Chem. B 2019, 123, 10131−10141